Hue University Journal of Science: Natural Science
Vol. 130, No. 1B, 43–51, 2021

pISSN 1859-1388
eISSN 2615-9678

NUMERICAL SIMULATION OF ALL-NORMAL DISPERSION VISIBLE TO NEAR-INFRARED SUPERCONTINUUM GENERATION IN PHOTONIC CRYSTAL FIBERS WITH CORE FILLED CHLOROFORM

Thi Minh Ngoc Vo[1], Dinh Quang Ho[2], Tung Thanh Le[3], Thi Gai Le[4], Canh Trung Le[1], Van Lanh Chu[1], Thuy Nguyen Thi[5], Van Thuy Hoang[1], Thanh Danh Nguyen[6], Van Hieu Le[3]*

[1] Department of Physics, Vinh University, 182 Le Duan St., Vinh City, Nghe An, Vietnam
[2] School of Chemistry, Biology and Environment, Vinh University, 182 Le Duan St., Vinh City, Nghe An, Vietnam
[3] Faculty of Natural Sciences, Hong Duc University, 565 Quang Trung St., Thanh Hoa City, Thanh Hoa, Vietnam
[4] Lam Son High School, 307 Le Lai St., Thanh Hoa City, Thanh Hoa, Viet Nam
[5] University of Education, Hue University, 34 Le Loi St., Hue, Vietnam
[6] A Sanh High School, IaGrai District, Gia Lai, Vietnam

* Correspondence to Van Hieu Le <levanhieu@hdu.edu.vn>

(*Received: 14 March 2021; Accepted: 15 June 2021*)

Abstract. This study proposes a photonic crystal fiber made of fused silica glass, with the core infiltrated with chloroform as a new source of supercontinuum (SC) spectrum. We numerically study the guiding properties of the fiber structure in terms of characteristic dispersion and mode area of the fundamental mode. Based on the results, we optimized the structural geometries of the $CHCl_3$-core photonic crystal fiber to support the broadband SC generations. The fiber structure with a lattice constant of 1 μm, a filling factor of 0.8, and the diameter of the first-ring air holes equaling 0.5 μm operates in all-normal dispersion. The SC with a broadened spectral bandwidth of 0.64 to 1.80 μm is formed by using a pump pulse with a wavelength of 850 nm, 120 fs duration, and power of 0.833 kW. That fiber would be a good candidate for all-fiber SC sources as cost-effective alternative to glass core fibers.

Keywords: photonic crystal fiber, supercontinuum generation, chloroform, nonlinear optics

1 Introduction

Supercontinuum (SC) generations in all-normal dispersion fiber have been a subject of intense research because of their fascinating properties. They have been exploited in numerous study fields and promising applications, such as optical coherence tomography [1] and ultra-short pulse generation [2]. Unlike in the anomalous dispersion regime, the SC generated by pumping in the normal regime of dispersion is achieved through the Self-Phase Modulation (SPM) and Optical Wave Breaking (OWB) mechanisms [3]. Therefore, the SC generation in the normal dispersion region enables obtaining spectra with better pulse-to-pulse temporal coherence and flatness [4].

For broadband SC generation, numerous efforts have been devoted to extending the spectral width and flatness over wavelength broadband. To achieve this, the photonic crystal fiber (PCF) requires special optical-wave-guiding designs to produce both flat all-normal dispersion and high-nonlinearity properties. Besides, the

initial laser pulse properties should be optimized in terms of pump wavelength, pulse duration, and input energy [5-6]. Various complicated designs, such as different core geometries [7] and multiple air-hole diameters in different rings [8], have been exploited to achieve ultra-flattened dispersion values. Meanwhile, high nonlinear values could be obtained with the use of greater-nonlinearity glasses other than silica, such as chalcogenide [9] and tellurium chalcogenide [10].

Another method for achieving materials with high nonlinear values is using hollow-core PCF filled with liquids. Much of effort has been concentrated on some liquids with high nonlinear coefficients, such as carbon disulfide (CS_2) [11], toluene (C_7H_8) [12], carbon tetrachloride (CCl_4) [13], ethanol (C_2H_5OH) [14], nitrobenzene ($C_6H_5NO_2$) [15], and water [16]. Since the selected liquids cause such a tremendous relative index difference, it is possible to observe and control the nonlinear effects as SC generation [11-14]. The obtained results indicate that it is possible to shift the zero-dispersion wavelength (ZDW) and match it with the pump wavelength emitted by a high-power commercial laser, obtaining all-normal and flat dispersion regime of expected spectral [17-18]. Liquids have been used for applications in the near or mid-infrared wavelength range [9, 10, 12-14]. In the meantime, the violet-visible range gets little attention although it contributes to various applications, such as fluorescence imaging, thermal sensing, photodynamic therapy, microscopy of cells, and tissue organization [19, 20].

Among the liquids mentioned above, chloroform ($CHCl_3$) emerges as an attractive candidate for the development of liquid PCFs because $CHCl_3$ has a high nonlinear refractive index (6.17×10^{-19} m^2/W – higher than that of fused silica, even up to 30 times) [21]. This nonlinearity enables the PCF to generate a much broader spectrum with low input power and within a short propagating distance [12, 15]. Another advantage of $CHCl_3$ is the transparent window in the visible to near-IR (0.5–1.6 μm) range [22] and its moderate toxicity compared with other liquids, such as CS_2 and C_7H_8 [23]. Furthermore, the refractive index of $CHCl_3$ is very close to that of fused silica. Therefore, it would be easy to design single-mode chloroform-filled core silica PCFs with a core size similar to that of standard silica fibers.

In this report, we numerically study the PCFs made of fused silica, with the core infiltrated with $CHCl_3$ as propagating media for the SC generation. The dispersion properties are optimized by modifying photonic parameters, i.e., filling factor and diameter of the first-ring air holes in the PCF structure, to obtain the all-normal dispersion flatness and the location of ZDW in the analyzed wavelength range. We utilize the generalized nonlinear Schrödinger equation (GNLSE) to demonstrate the SC generation for that optimum fiber structure. We also discuss the advantages of the selected PCF.

2 Modeling PCF structure and the study method

The cross-section of the $CHCl_3$-filled PCF is depicted in Fig. 1.

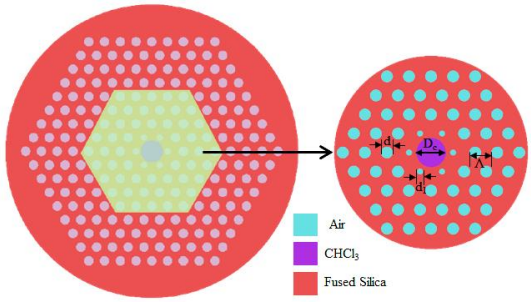

Fig. 1. The cross-section of modelled PCF, where D_c is the diameter of the $CHCl_3$-core

pISSN 1859-1388
eISSN 2615-9678

The PCF background material in this study is fused silica. The cladding air-holes are arranged in a hexagonal lattice with diameter d (μm) and lattice pitch Λ (μm). Besides, the diameter of the first-inner-ring air holes is d_1 (μm), and it has a significant contribution to the dispersion properties. There are eight air-holes rings in this designed PCF structure, and they are large enough for the change in the dispersion of the PCF to be negligible if one more ring on the outer cladding is added. The center air hole with the diameter D_c (2 × Λ − 1.2 × d) is filled with high-nonlinear liquid $CHCl_3$ represented by pink color.

The refractive indices of the materials as a function of wavelength are given in the Sellmeier equation as

$$n(\lambda) = \sqrt{1 + \frac{B_1\lambda^2}{\lambda^2 - C_1} + \frac{B_2\lambda^2}{\lambda^2 - C_2} + \frac{B_3\lambda^2}{\lambda^2 - C_3}} \quad (1)$$

where the B_i and C_i (μm²) are Sellmeier's coefficients given in Table 1 [22].

The propagation of the optical pulse whose field amplitude changes slowly is described by using the generalized nonlinear Schrödinger equation [24]

$$\frac{\partial A}{\partial z} + \frac{\alpha}{2}A + \sum_{n=2}^{\infty} i^{(n-1)}\frac{\beta_n}{n!}\frac{\partial^n A}{\partial t^n} = i\gamma\left(1 + \frac{i}{\omega_0}\frac{\partial}{\partial t}\right)A(z,t)\left[\int_{-\infty}^{\infty} R(t')|A(z,(t-t')|^2 dt'\right] \quad (2)$$

where z is the spatial coordinate along the fiber; α is the total fiber loss, and β_n is the n-th order of dispersion.

Table 1. The coefficients of fused silica and chloroform

Sellmeier coefficients	Materials	
	Fused silica	$CHCl_3$
B_1	0.6694226	1.50387
C_1 (μm²)	4.4801×10^{-3}	3.049×10^{-2}
B_2	0.6694226	0.00345
C_2 (μm²)	1.3285×10^{-2}	0.15207
B_3	0.8716947	–
C_3 (μm²)	95.341482	–

The terms on the right-hand side of Eq. (2) represent nonlinearity in the fiber and include contributions from the Kerr effect and Raman effect. Specifically, the Kerr nonlinear parameter γ of the fiber is defined as [24]

$$\gamma(\lambda) = \frac{2\pi n_2}{\lambda A_{eff}} \quad (3)$$

where A_{eff} is the effective cross-sectional area of the fiber, and n_2 is the nonlinearity of $CHCl_3$.

The effective area A_{eff} is computed from [24]

$$A_{eff} = \frac{\left(\iint |E|^2 dxdy\right)^2}{\iint |E|^4 dxdy} \quad (4)$$

where $E(x, y)$ is the field distribution of the fiber mode.

The other nonlinear term in Eq. (2) represents the Raman response. It should contain the main contributions as the electronic and vibrational part. Take the suppose that the electronic factor contributes instantaneously, the Raman response function $R(t)$ can be written as

$$R(t) = (1 - f_R)\delta(t) + f_R h_R(t) \quad (5)$$

where $\delta(t)$ is the Dirac delta function, and f_R represents the fractional contribution of the delayed Raman response function $h_R(t)$, which, in turn, takes an approximate analytical form

$$h_R(t) = \frac{\tau_1^2 + \tau_2^2}{\tau_1\tau_2^2}\exp(-t/\tau_2)\sin(-t/\tau_1) \quad (6)$$

where τ_1 = 4.378 fs; τ_2 = 0.27 ps; f_R is equal to 0.35 for $CHCl_3$ [25, 26].

In the simulation of SC generation, we use the split-step Fourier method to solve the GNLSE in both the time and the frequency domains for input femtosecond pulses. The analysis is simulated with the following parameters: fiber length 10 cm, Gaussian-shaped pulse 120 fs, the nonlinear refractive index of $CHCl_3$ n_2 = 6.17 × 10^{-19} (m²/W), and pump wavelength 850 nm. The simulation domain consists of 8192 grid points over a time duration of 1.5 ps.

3 Numerical results

In our study, we aim at designing a new air-glass structure of photonic cladding that allows for flat slopes and low chromatic dispersion inside the all-normal regime, which is employed for supercontinuum source at pumping of 850 nm. We analyze how the geometrical factors of the structure, namely the lattice constant and filling factor, influence the PCF's linear properties, particularly the effective dispersion for precise shaping and a wide range of wavelengths in the all-normal regime.

Numerical simulations are performed by using Lumerical Mode Solution software [27]. In all investigated cases, we only consider the PCF's fundamental mode, as shown in Fig. 2.

To optimize the structure, we first simulate the influence of the filling factor f in the range of 0.4–0.9 with the lattice pitch equal to 1.0 μm. The resulting dispersion curves for the fundamental modes are depicted in Fig. 3. Increasing the filling factor leads to an increase in the difference between the maximum and minimum dispersion values and also can move the dispersion region from normal to anomalous.

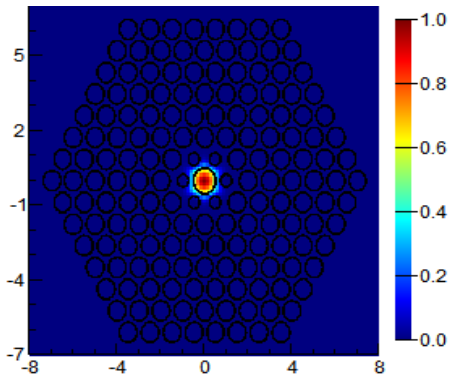

Fig. 2. Numerically calculated intensity distribution of the fundamental mode of the PCF

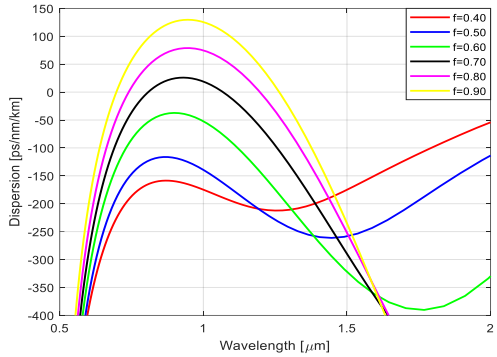

Fig. 3. Characteristics of the fundamental mode dispersion with different filling factors with lattice pitch equal to 1.0 μm

In the second step, based on the reported results in [28], we reduce the diameter of the first-ring air holes. This reduction causes the dispersion to shift from the anomalous to the normal region and increases the flat dispersion. Thus, the filling factor in the further analysis is 0.7, 0.8, and 0.9.

Figures 4a–c depict the dispersion characteristics for different diameters of the first-ring air holes with each filling factor. Reducing the diameter of air holes on the first row leads the dispersion to move down and increases the flat dispersion properties. Meanwhile, Fig. 4d shows the dispersion characteristics for different filling factors when the diameter of the first-ring air holes is constant. When the filling factor increases, the dispersion slope shifts toward the anomalous dispersion area from the normal dispersion area, and the peak of the dispersion curve moves to longer wavelengths.

On the basis of initial numerical investigations, we select a fiber with following parameters: Λ = 1.0 μm; f = 0.8, and d_1 = 0.5 μm. This fiber has optimum dispersion characteristics for SC generation because it has all-normal dispersion, and the dispersion slope is flat. This fiber also has a maximum-point wavelength closest to the pumping wavelength.

pISSN 1859-1388
eISSN 2615-9678

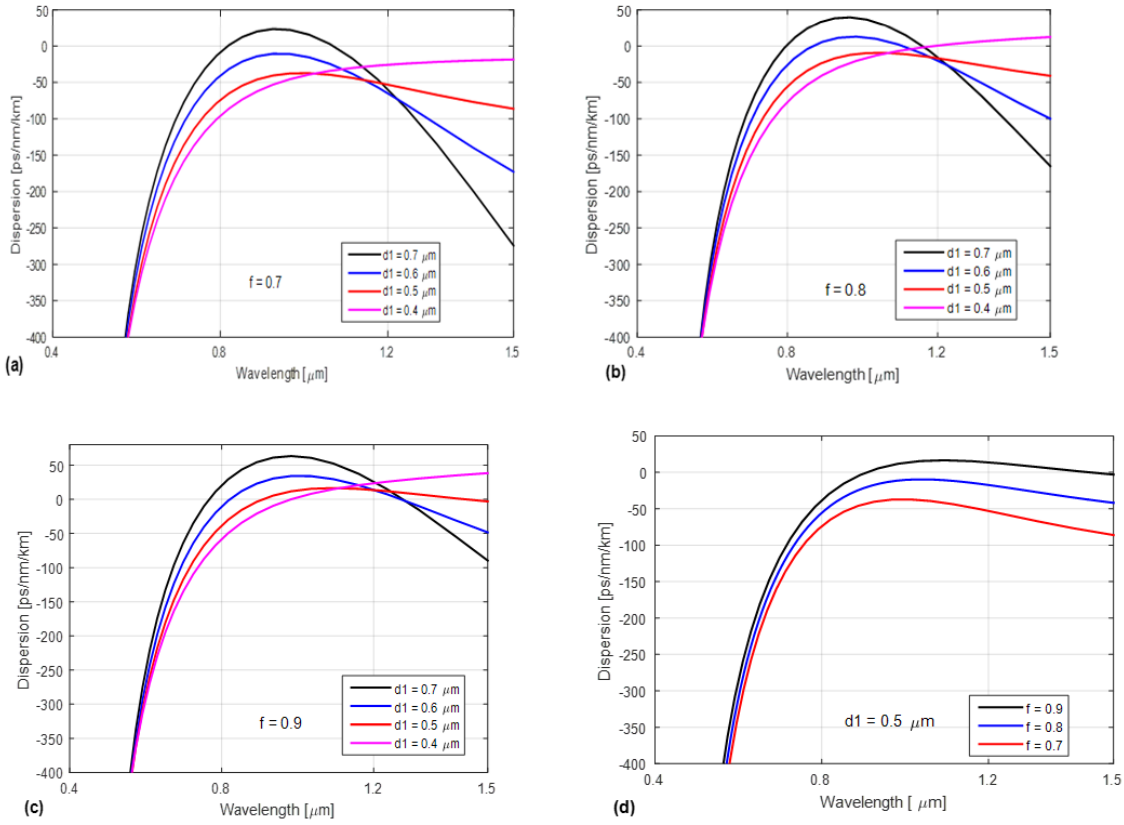

Fig. 4. Characteristics of the fundamental mode dispersion with different diameters of the air holes on the first row and various filling factor

In addition, the optimal fiber structure without changing the diameter of the first-ring air holes is characterized by anomalous dispersion where the first ZDW is 0.72 μm; the second ZDW is 1.24 μm, and the dispersion at the 0.85 μm wavelength equals 66.86 ps/nm/km (Fig. 5a).

Fig. 5b shows the effective modal area and nonlinear coefficients of the optimal structure. The modal area of the fundamental mode increases with the wavelength. Because the core diameter is relatively small, it also leads to a small effective modal area of the optimal structure. For the wavelength of 850 nm, the modal area equals 1.8375 μm^2, while nonlinear coefficients equal 650.942 W^{-1}·km^{-1}.

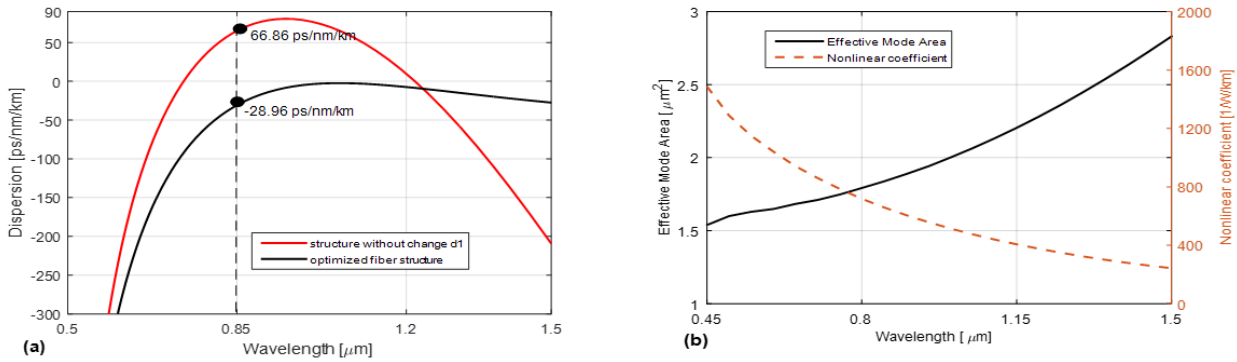

Fig. 5. (a) Optimal dispersion properties and (b) Effective modal area and nonlinear coefficient of the optimized PCF

Fig. 6 shows the output supercontinuum spectra under different powers at the length 10 cm. With an increasing pump power, the spectrum of the supercontinuum source broadens obviously, especially the infrared part of the spectrum. Besides, $CHCl_3$ has high absorption when wavelengths are less than 0.5, so the output spectrum is limited in this region. For a pump power of 0.833 kW, a wide supercontinuum spectrum ranging from 640 to 1800 nm is obtained after propagating about 10 cm inside the PCF.

Fig. 7 depicts the spectral of the pulse along the propagation distance with various powers. Meanwhile, Fig. 8 shows the spectral and temporal evolution of the pulse along the propagation distance with an input power of 0.833 kW. Here, the pump wavelength is located inside the normal-dispersion area, after the initial widening of the spectrum due to phase self-modulation, which is characterized by temporal spectrogram in an S-shape, as shown in Fig. 8b. Next, we observe a further widening of the spectrum in the short-wavelength range due to OWB. As presented in Fig. 8a, the OWB first occurs in the trailing edge of the pulse at 1.15 cm of propagation and generates a new wavelength band around 0.7 μm. On the leading edge, the OWB occurs only after a 4.0 cm distance of the propagation and creates a new wavelength band around 1.1 μm. For further propagation, the broad spectrum is asymmetric, with a larger broadening on the long-wavelength side as the propagation distance increases. It is clear that because different frequency components usually have different velocities, the time delay between different frequencies becomes larger with longer propagation, as shown in Fig. 8c.

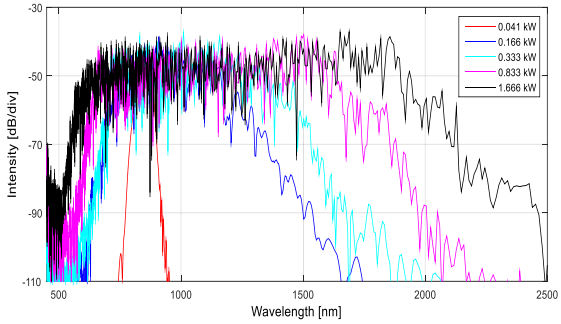

Fig. 6. SC spectrum calculated at distance of 10 cm when pumped with pulses of 120 fs duration, 850 nm pump wavelength and different powers

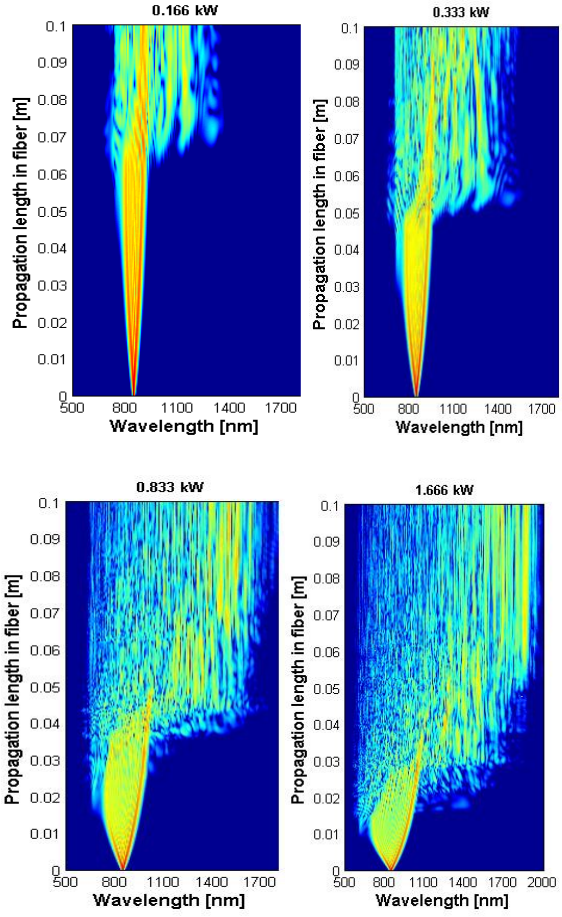

Fig. 7. Numerical calculations of the spectral of the pulse along the fiber in $CHCl_3$ filled-core PCF

pISSN 1859-1388
eISSN 2615-9678

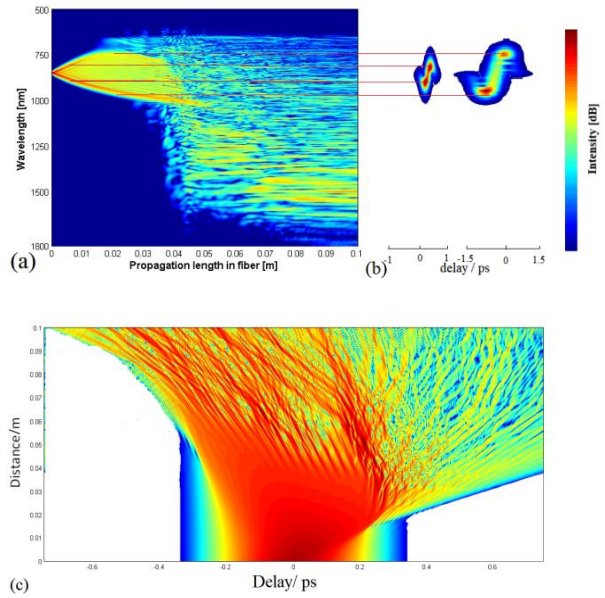

Fig. 8. Numerical calculations of the spectral (a) and temporal evolution (b) and (c) of the pulse along the fiber in $CHCl_3$ -filled core PCF

4 Conclusion

In this paper, we present a numerical study on the optimum structure of a PCF made of fused silica with a $CHCl_3$-filled core for obtaining all-normal dispersion characteristics. The fiber structure is selected to achieve flat dispersion, low dispersion, the local pump wavelength, and the SC generation in the all-normal dispersion regime with pumping at 850 nm. According to the conducted simulations, the optimized fiber with the following characteristics: lattice constant Λ = 1.0 μm; filling factor f = 0.8, and d_1 = 0.5 μm, exhibits an all-normal dispersion, and its peak equals –28.96 ps/nm/km at 850 nm.

Our numerical simulation results demonstrate that in the $CHCl_3$-filled-core optimal PCF structure, the SC with a broadened spectral bandwidth of 640 to 1800 nm is generated by a pump pulse with a central wavelength of 850 nm, 120 fs duration, and power of 0.833 kW. Further increasing the width of the spectral can be expected if we increase input pulse energy. Furthermore, high nonlinearity makes chloroform a good candidate as a nonlinear medium for use in highly nonlinear liquids-core PCFs. Therefore, this fiber structure would be a good candidate for all-fiber SC sources as a cost-effective alternative to glass-core fibers. Additionally, the linear refractive index of $CHCl_3$ is only about 0.012 lower than that of silica. The latter allows for the design of single-mode $CHCl_3$-filled-core-silica PCFs, which have a core size similar to that of standard silica fibers.

Funding statement

This research is funded by Vietnam National Foundation for Science and Technology Development (NAFOSTED) under grant number 103.03-2020.19.

References

1. Povazay B, Bizheva K, Unterhuber A, Hermann B, Sattmann H, Fercher AF, et al. Submicrometer axial resolution optical coherence tomography. Optics Letters. 2002;27(20): 1800-1802.
2. Heidt AM, Rothhardt J, Hartung A, Bartelt H, Rohwer EG, Limpert J, et al. High quality sub-two cycle pulses from compression of supercontinuum generated in all-normal dispersion photonic crystal fiber. Optics Express. 2011;19(15): 13873-13879.
3. Heidt AM, Hartung A, Bosman GW, Krok P, Rohwer EG, Schwoerer H, et al. Coherent octave spanning near-infrared and visible supercontinuum generation in all-normal dispersion photonic crystal fibers. Optics Express. 2011;9(4):3775-3787.
4. Stepniewski G, Klimczak M, Bookey H, Siwicki B, Pysz D, Stepien R, et al. Broadband supercontinuum generation in normal dispersion all-solid photonic crystal fber pumped near 1300 nm. Laser Physics Letter. 2014;11(5):055103.
5. Medjouri A, Abed D, Ziane O, Simohamed LM. Design and optimization of As_2S_5 chalcogenide channel waveguide for coherent mid-infrared

supercontinuum generation. Optik. 2018;154(2018): 811-820.

6. Hansen KP. Dispersion flattened hybrid-core nonlinear photonic crystal fiber. Optics Express. 2003;11(13):1503-1509.
7. Saitoh K, Florous NJ, Koshiba M. Theoretical realization of holey fiber with flat chromatic dispersion and large mode area: an intriguing defected approach. Optics Letters. 2006;31(10):26-28.
8. Poletti F, Finazzi V, Monro TM, Broderick NGR, Tse V, Richardson DJ. Inverse design and fabrication tolerances of ultra-flattened dispersion holey fibers. Optics Express. 2005;13(10):3728-3736.
9. Balani H, Singh G, Tiwari M, Janyani V, Ghunawat AK. Supercontinuum generation at 1.55 μm in As_2S_3 core photonic crystal fiber. Applied Optics. 2018;57(13): 3524-3533.
10. Jiao K, Yao J, Zhao Z, Wang X, Si N, Wang X, et al. Mid-infrared flattened supercontinuum generation in all-normal dispersion tellurium chalcogenide fiber. Optics Express. 2019;27(3):2036-2043.
11. Churin D, Nguyen TN, Kieu K, Norwood RA, Peyghambarian N. Mid-IR supercontinuum generation in an integrated liquid-core optical fiber filled with CS_2. Optics Material Express. 2013;3(9):1358-1364.
12. Hoang VT, Kasztelanic R, Anuszkiewicz A, Stepniewski G, Filipkowski A, Ertman S, et al. All-normal dispersion supercontinuum generation in photonic crystal fibers with large hollow cores infiltrated with toluene. Optics Material Express. 2018;8(11):2159-3930.
13. Hoang VT, Kasztelanic R, Filipkowski A, Stepniewski G, Pysz D, Klimczak M, et al. Supercontinuum generation in an all-normal dispersion large core photonic crystal fiber infiltrated with carbon tetrachloride. Optics Material Express. 2019;9(5): 2159-3930.
14. Van HL, Long VC, Nguyen HT, Nguyen AM, Buczynski R, Kasztelanic R. Application of ethanol infiltration for ultra-flatted normal dispersion in fused silica photonic crystal fibers. Laser Physics. 2018;28(11):115106.
15. Van LC, Hoang VT, Long VC, Borzycki K, Xuan KD, Quoc VT, et al. Supercontinuum generation in photonic crystal fibers infiltrated with nitrobenzene. Laser Physics. 2020; 30(3):035105.
16. Canh TL, Hoang VT, Van HL, Pysz D, Long VC, Dinh TB, et al. Supercontinuum generation in all-normal dispersion suspended core fiber infiltrated with water. Optical Materials Express. 2020;10(7):1733-1748.
17. Pniewski J, Stefaniuk T, Van HL, Long VC, Van LC, Kasztelanic R, et al. Dispersion engineering in nonlinear soft glass photonic crystal fibers infiltrated with liquids. Applied Optics. 2016;55(19):5033-5040.
18. Van HL, Buczynski R, Long VC, Trippenbach M, Borzycki K, Nguyen AM, et al. Measurement of temperature and concentration influence on the dispersion of fused silica glass photonic crystal fiber infiltrated with water-ethanol mixture. Optics Communications. 2018;407:417-422.
19. He J, Chen H, Hu J, Zhou J, Zhang Y, Kovach A, et al. Nonlinear nanophotonic devices in the ultraviolet to visible wavelength range. Nanophotonics. 2020;9(12):3781-3804.
20. Bozolan A, de Matos CJS, Cordeiro CMB, dos Santos EM, Travers J. Supercontinuum generation in a water-core photonic crystal fiber, Optics Express. 2008;6(13):9671-9676.
21. Karasawa N. Dispersion properties of liquid-core photonic crystal fibers. Applied Optics. 2012;51(21): 5259-5265.
22. Kedenburg S, Vieweg M, Gissibl T, Giessen H. Linear refractive index and absorption measurements of nonlinear optical liquids in the visible and near-infrared spectral region. Optical Materials Express. 2012;2(1):1588-1611.
23. Van LC, Anuszkiewicz A, Ramaniuk A, Kasztelanic R, Xuan KD, Long VC, et al. Supercontinuum generation in photonic crystal fibres with core filled with toluene. Journal off Optics. 2017;19(12):125604.
24. Agrawal GP. Nonlinear fiber optics. Springer. 2000.
25. Lee S, Jen M, Pang Y. Twisted Intramolecular Charge Transfer State of a "Push-Pull" Emitter. International Journal of Molecular Sciences. 2020;21(21):7999.
26. Wanga C, Lia W, Lia N, Wang W. Numerical simulation of coherent visible-to-near-infrared supercontinuum generation in the $CHCl_3$-filled photonic crystal fiber with 1.06 μm pump pulses, Optics & Laser Technology. 2017;88(2017):215-221.
27. Ansys Canada Ltd. Lumerical Mode Solutions. Version 7.12.1731. Vancouver: Ansys Canada Ltd; 2021.

pISSN 1859-1388
eISSN 2615-9678

28. Stępniewski G, Pniewski J, Pysz D, Cimek J, Stępień R, Klimczak M, et al. Development of dispersion-optimized photonic crystal fibers based on heavy metal oxide glasses for broadband infrared supercontinuum generation with fiber lasers. Sensors (Basel). 2018;18(12):4127.